Supplementary Information for

Mesoscale Modelling of Fibrin Clots: The Interplay between Rheology and Microstructure at the Gel Poin

S1 Supplementary Equations

The thermal fluctuation is included in the model by

$$m\mathrm{d}\tilde{\mathbf{v}}_i = \sum_j \left(A_{ij}\mathrm{d}\overline{\mathbf{W}}_{ij} + B_{ij}\frac{1}{D}\mathrm{tr}[\mathrm{d}\mathbf{W}_{ij}] \right) \cdot \mathbf{e}_{ij}, \tag{S1}$$

where $\overline{\mathbf{W}}_{ij}$ is a matrix of independent increments of a Wiener process for each pair i, j of particles, and $\overline{\mathbf{W}}_{ij}$ is its traceless symmetric part, given by

$$\mathrm{d}\overline{\mathbf{W}}_{ij} = \frac{1}{2}\left[d\mathbf{W}_{ij} + \mathrm{d}\mathbf{W}_{ij}^T \right] - \frac{\delta^{\alpha\beta}}{D}\mathrm{tr}[\mathrm{d}\mathbf{W}_{ij}],$$

where D is the system dimensionality. To satisfy the fluctuation-dissipation balance the amplitude of the thermal noises A_{ij} and B_{ij} are related to the friction coefficients a and b through

$$A_{ij} = \left[4k_B T a \frac{F_{ij}}{\rho_i \rho_j} \right]^{1/2}, \tag{S2}$$

$$B_{ij} = \left[4k_B T \left(b - a\frac{D-2}{D} \right) \frac{F_{ij}}{\rho_i \rho_j} \right]^{1/2}, \tag{S3}$$

To describe the variation of the pressure with the density of the system we adopt the Cole equation (a.k.a. Tait's equation of state) given by $p_i = c^2\rho_0/7\left[(\rho_i/\rho_0)^7 - 1\right] + p_b$ (S4) where c is the speed of sound on the fluid, and ρ_0 is the reference density. The term $c^2\rho_0/7$ corresponds to the reference pressure of the system, given by $c^2 = \partial p/\partial\rho|_{\rho=\rho_0}$. The parameter p_b is a background pressure that provides numerical stability by always keeping the system's pressure positive.

We adopt the Lucy kernel[1] typically used in SDPD for the interpolant function,

$$W(r) = \begin{cases} \frac{w_0}{h^D}\left(1 + \frac{3r}{h}\right)\left(1 - \frac{r}{h}\right)^3, & r/h < 1. \\ 0, & r/h > 1, \end{cases} \tag{S5}$$

where $w_0 = 5/\pi$ or $w_0 = 105/16\pi$ for two or three dimensions, respectively. The reader is referred to[2] for a comprehensive description of the SDPD method.

S2 Fractal dimension evaluation

Fractal geometry as a tool for assessing the intricacy of natural formations introduced by Mandelbrot.[3] When an item exhibits self-similarity across different length scales, denoted as scale-free behavior, it qualifies as a fractal. This characteristic is governed by power-law functions featuring a singular exponent, leading to a non-integer dimension termed D_f. In cluster analysis, the computation of D_f from the radius of gyration (R_g) involves a linear fit to $R_g \sim M^\beta$ on a log-log scale. Here, $D_f = 1/\beta$ is the estimated fractal dimension. We calculate the radius of gyration R_g of a cluster using $R_g^2 = 1/M_A\sum_{i=1}^{M_A}(r_i - r_{cm})^2$, where r_i is the position of ith particle and r_{cm} is the center of mass of the cluster.

As particle volume fraction increases, the fractal dimension is expected to increase, approaching 3 when the volume fraction is 1.[4] Therefore, we limit our maximum concentration to $\phi_{int} = 15\%$, which gives us $D_f > 2$. Also, the fractal model can only be applied to particle volume fractions less than 20%. At higher volume fractions, the number of particles per cluster becomes so small that using a fractal model, and hence power law dependencies, is no longer justified.[4]

S2.1 Fractal Dimension at Gel Point

Some studies[5] calculate the value of D_f from analysis of the viscoelastic data at the *GP* by the established relationship of Muthukumar for the incipient gel network ($D_f = (10\alpha - 15)/(2\alpha - 6)$ for 3D space).[6] We use a numerical measure of the gel microstructure. The percolation theory defines the polymerizing system as macroscopically homogeneous on a length scale $L >> \varepsilon$. In contrast, for $L << \varepsilon$ the sample-spanning network cluster is a 'self-similar' or fractal object. The blob-like network structure of gels has a profound impact on their features. A uniform distribution of particles is seen when the concentration of particles inside a blob is equal to the concentration of particles across the gel.

S3 Simulation Details

We conducted numerical simulations using the clustering aggregation framework (based on the smoothed dissipative particle dynamics method SDPD) previously introduced.[7] We focus our investigations on periodic three-dimensional systems and consequently reported clusters with characteristic D_f ranging from $1.56 \pm 0.1 - 2.18 \pm 0.04$. Since the formed gel spans the whole simulation domain, which is periodic, we used an arbitrary boundary condition[8] approach for imposing the shear rate in SAOS (see S4). The characteristic parameters of the SDPD method are shown in the Table.S1. Simulations were performed using the software LAMMPS modified to incorporate the SDPD model.[9,10] To account for the influence of the randomness of the bonding process, all the simulations are conducted over five realizations, initialized with different positions and velocities, in addition, we computed the standard deviation of all reported results.

We use dimensionless parameters in our SDPD simulations. Thus, we consider characteristic length (L_{sdpd}), mass (m_{sdpd}), and time (τ_{sdpd}) units. The size of the interpolation kernel h, for an adequate estimation of hydrodynamic interactions, is chosen as $4dx = 0.8L_{\mathrm{sdpd}}$. Bond distances ($r_0 = 0.25L_{\mathrm{sdpd}} = 1.25dx$) are defined to be close to the equilibrium interparticle distance (dx) to avoid artificial density variations. By adjusting the bond distance, we tune the elasticity modulus of the gels, calibrating the power low slope of the elasticity modulus at the gel point. The chosen bond distance value directly affects our simulation's power-law slope and the elasticity modulus values. A smaller bond distance generally leads to tighter bonding between particles, with a higher elasticity modulus. In contrast, increasing the bond distance allows for a more flexible gel, which may lower the elasticity modulus. The bonding criteria $r^* = 0.4L_{\mathrm{sdpd}} < h$ is fixed to ensure attainable gelling kinetics, within the simulation time modeled, avoiding artificial long-range interactions. We consider bond strength,

and stiffness parameter as $D_{Morse} = 300[m_{\text{sdpd}} L_{\text{sdpd}}^2 \tau_{\text{sdpd}}^{-2}]$ and $\alpha = 1[L_{\text{sdpd}}]^{-1}$. We define the mass density as $\rho = 1[m_{\text{sdpd}}]/[L_{\text{sdpd}}]^3$. The equilibrium particle density is $d_i = 1/dx^3[1/L_{\text{sdpd}}^3]$, whereas the mass per particle is $m_0 = 0.008[m_{\text{sdpd}}]$ and the viscosity $\eta = 10[m_{\text{sdpd}} L_{\text{sdpd}} \tau_{\text{sdpd}}]^{-1}$. We set the $k_B T = 10^{-6}[m_{\text{sdpd}} L_{\text{sdpd}}^2 \tau_{\text{sdpd}}^{-2}]$ to reduce the thermal fluctuation and minimize the noise-to-signal ratio during the stress measurements in SAOS. dt considered as $dt < min(0.25h/c_s, 0.125h^2/\nu)$.[11] Thus, the size of the time steps was fixed on $10^{-4}\tau_{\text{sdpd}}$ to ensure lower density fluctuation.

For our SAOS study, we define the simulation time for each frequency as the period required for the G' and G'' to reach steady-state values. This stabilization typically occurs within approximately 10 cycles at each frequency. We apply averaging over the last 5 cycles to ensure consistent results. The window time for gel formation is the time needed to reach the final gel state, where no bonds are being created, indicating that the network has stabilized.

S4 Arbitary boundary conditions for imposing shear

We use the proposed boundary conditions by Moreno and Ellero.[8] This approach is suitable for conducting rheological studies where rheological characterization can be conducted using arbitrary flow types (simple shear, extensional, mixed flow) in periodic simulation domains. They adopt a domain decomposition scheme that considers the system made by a core region (where the stress is measured), a boundary condition region (where the characteristic type of flow is imposed), and buffer regions (that stabilize the system). We use buffer regions that expand over two-fold the size of the interpolation kernel to ensure the system's stability and simulate up to a satisfactory agreement the properties of the fluid.[8] These boundary conditions are suitable for applying the oscillatory shear over the gels percolating the simulation domain. In the Fig. S1 sketch of the regions defined for SDPD simulations, the type of boundary conditions defined according to the target velocity field is shown. Parameters used for boundary conditions are shown in the Table. S2 according to the study we do in the next section.

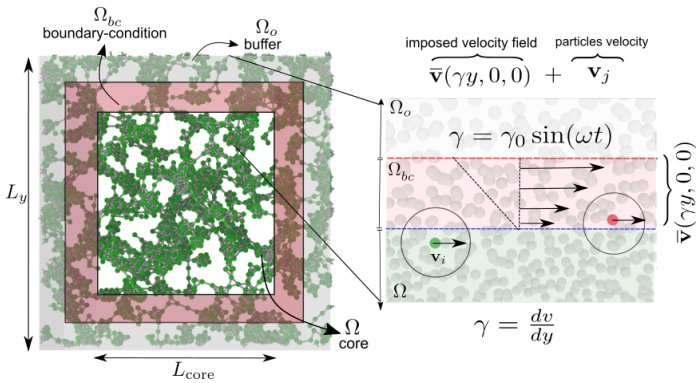

Fig. S1 Sketch of the regions defined for SDPD simulations, and the type of boundary conditions defined according to the target velocity field. The interpolated velocity field acts over particles in Ω_{bc}.[8]

S4.1 Box-size dependency study for arbitrary boundary condition in the SAOS measurements

For implementing the arbitrary boundary condition, based on the findings of Moreno and Ellero[8], configuring the core size and buffer zone is essential for optimizing boundary conditions in SDPD under pure shear simulations. They showed a core size, L_{core} of approximately $\geq 5h$ (h is the kernel cutoff radius) is effective for accurately reproducing flow characteristics. They indicate that maintaining a $L_{buffer}/L_{core} > 0.1$ allows the buffer zone to function effectively as a transitional region, minimizing boundary layer artifacts by smoothing interactions between adjacent areas. To investigate the stability and precision of SAOS simulations in our finite domains boundary condition, we test various core sizes, $L_{core} = 4.5h, 5h, 5.5h$, fixed $L_{buffer} = L_{bc} = 0.25L_{core}$ and for 2 gel states with high and moderate G' slope, (Branched mechanism at the final gel state and Highly-Connected mechanism at a state above the gel point). Table. S3, compares the slopes of G' and G'' for the 3 core sizes. We select $L_{core} = 5h$ for SAOS simulations. Using the lower limit for L_{core}=$5h$ comparing L_{core}=$5.5h$ creates a smaller gap (core size), lower Reynolds number, and therefore lower inertial effect, supporting a wider range of shear rates. It has also sufficient precise results comparing the lower size, L_{core}=$4.5h$.

S5 Stress measurements and fluid inertia effect in oscillatory rheometry

We compute shear stresses on the core region (see arbitrary boundary conditions) of the simulation domain. With measured stress, we extract G'' and G'. For small-amplitude oscillatory shear, the stress response is also sinusoidal, but delayed by a phase delay, δ ($\sigma(t) = \sigma_0 sin(\omega t + \delta)$). We extract G'' and G' by using the sine sum identity equation: $\sigma(t) = \sigma_0 sin(\omega t) cos(\delta) + \sigma_0 cos(\omega t) sin(\delta)$. Then measured as $G'' = \sigma_0/\gamma_0 sin(\delta)$ and $G' = \sigma_0/\gamma_0 cos(\delta)$. The total viscous stress measured σ includes contributions from both the solvent and the gel. However, to account only for the stress contributions associated with gel-gel and solvent-gel interactions, we subtract the viscous stress attributable to the solvent ($\sigma(1-\phi_{gel})$) from the total viscous part and keep the part of the gel. Here, ϕ_{gel} corresponds to the actual volume fraction of the gel (or active particles) at the time of stress measurement. We must note that in our simulations the control parameter is the initial concentration ϕ_{int}, which in principle may not coincide with the final gel fraction, depending on the degree of conversion of passive to active particles. This difference occurs because, at the gel point, some **P** particles may remain.

It has been previously identified,[12] that spurious measurements in the stress at high frequencies and large gaps can emerge due to inertial effects. Since those effects are ubiquitous in numerical simulations, we subtract the apparent elastic modulus ($\rho\omega^2 s^2/6$) from the measured G'. This artificial term does not describe any rheological property and is composed of fluid density ρ, frequency ω, and gap width s, reflecting the influence of fluid inertia.[12]

S6 Supplementary Tables

Table S1 Input parameters of the SDPD method

Domain size $[L_x \times L_y \times L_z]$	$(40dx)\times(40dx)\times(40dx)$
Total number of particles (N_t)	64000
Mass(m)	0.008
viscosity(η)	10
k_BT	0.000001
Density(ρ_0)	1
Pressure(p_0)	0
Speed of sound (c_s)	50
Time step (dt)	10^{-4}
Initial lattice spacing(dx)	0.2
Cutoff radius (h)	$4dx$

Table S2 Parameters of arbitrary boundary condition

L_{core}	$(5h)$
L_y	$(10h)$

Table S3 Study the effect of L_{core} on G'' and G' slopes (in log scale) in arbitrary boundary condition method [8] for Branched and Highly-Connected mechanisms (above the gel point). (The maximum standard deviation is ± 0.03 for modules slopes)

Mechanisms	Core Sizes		
	$L_{core} = 4.5h$	$L_{core} = 5h$	$L_{core} = 5.5h$
Branched	$G'slope = 1.95$	$G'slope = 1.98$	$G'slope = 1.99$
	$G''slope = 1.0$	$G''slope = 1.01$	$G''slope = 1.02$
$Highly-Connected(above\,gel\,point)$	$G'slope = 0.40$	$G'slope = 0.43$	$G'slope = 0.43$
	$G''slope = 0.70$	$G''slope = 0.72$	$G''slope = 0.73$

References

1 P. Espanol and M. Revenga, *Physical Review E*, 2003, **67**, 026705.

2 M. Ellero and P. Español, *Applied Mathematics and Mechanics*, 2018, **39**, 103–124.

3 B. B. Mandelbrot, *New York*, 1983.

4 H. Wu and M. Morbidelli, *Langmuir*, 2001, **17**, 1030–1036.

5 P. A. Evans, K. Hawkins, R. H. Morris, N. Thirumalai, R. Munro, L. Wakeman, M. J. Lawrence and P. R. Williams, *Blood, The Journal of the American Society of Hematology*, 2010, **116**, 3341–3346.

6 M. Muthukumar, *Macromolecules*, 1989, **22**, 4656–4658.

7 E. Zohravi, N. Moreno and M. Ellero, *Soft Matter*, 2023, **19**, 7399–7411.

8 N. Moreno and M. Ellero, *Physics of Fluids*, 2021, **33**, 012006.

9 S. Plimpton, *Journal of computational physics*, 1995, **117**, 1–19.

10 M. Jalalvand, M. A. Charsooghi and S. Mohammadinejad, *Computer Physics Communications*, 2020, **255**, 107261.

11 J. J. Monaghan, *In: Annual review of astronomy and astrophysics. Vol. 30 (A93-25826 09-90), p. 543-574.*, 1992, **30**, 543–574.

12 G. Böhme and M. Stenger, *Journal of Rheology*, 1990, **34**, 415–424.